

Electronic Supporting Information

Non-crystal-RuO_x/crystalline-ZnO composites: controllable synthesis and high-performance toxic gas sensor

Na Luo, Haijie Cai, Xiaojie Li, Mengmeng Guo, Chen Wang, Pengfei Hu, Xiaohong

*Wang, Zhixuan Cheng, Jiaqiang Xu**

NEST Lab, Department of Physics, Department of Chemistry, College of Sciences,

Shanghai University, Shanghai 200444, China.

E-mail: xujiaqiang@shu.edu.cn (J. Xu)

Characterization

Crystal structure of the products was characterized by X-ray diffraction analysis (XRD, Rigaku Corp., D/max2500) by using Cu K α 1 radiation (40 mA, 40 kV, 6°/min from 20 to 80°). The morphologies of the samples were observed by a field emission scanning electron microscopy (FESEM, JSM-6700F). The morphologies of all the samples were observed by Transmission electron microscopy (TEM, JEOL Ltd., JEM-2100F) equipped with an energy dispersive X-ray spectroscopy (EDS). The chemical states of the surface elements were measured by X-ray photoelectron spectroscopy (XPS) (Thermo fisher scientific Ltd, ESCALAB 250Xi) by using an Al K α monochromated (150 W, 20 eV pass energy, 500 μ m spot size). The C 1s signal at 284.6 eV was used to calibrate the binding energy scale. The Raman spectra were obtained on a Renishaw spectrometer (Raman, INVIA). The composition of the Li and Ru was measured by the inductively coupled plasma atomic emission spectroscopy (ICP-AES, Agilent 725) and energy dispersive spectrometer (EDS). The redox performance of the materials were measured by H₂ temperature program reduction (H₂-TPR, AutoChem II 2920).

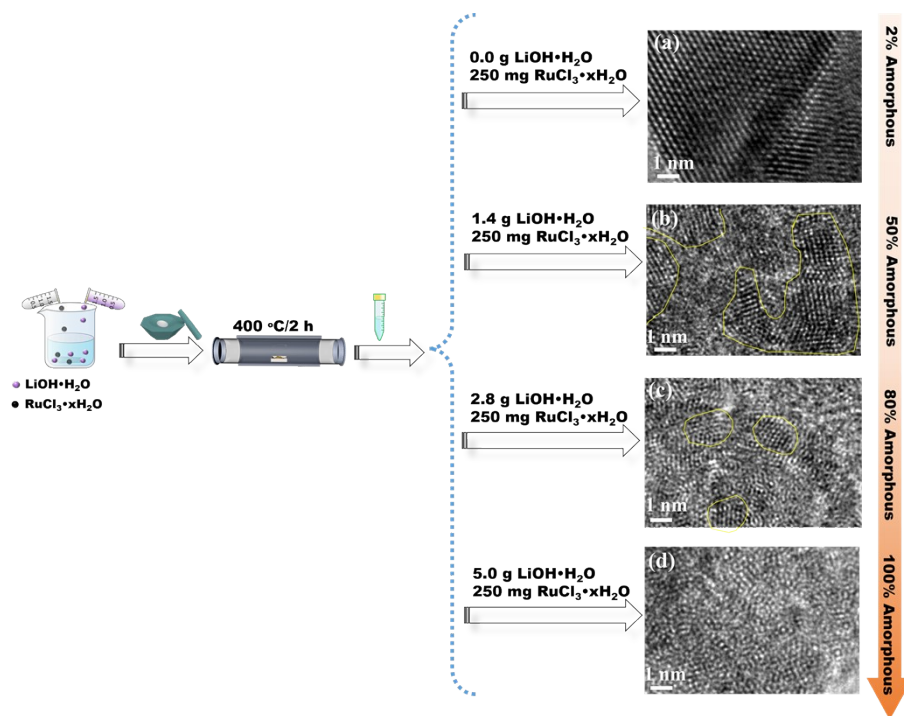


Fig. S1. Schematic illustration of the synthesis of RuO_x .

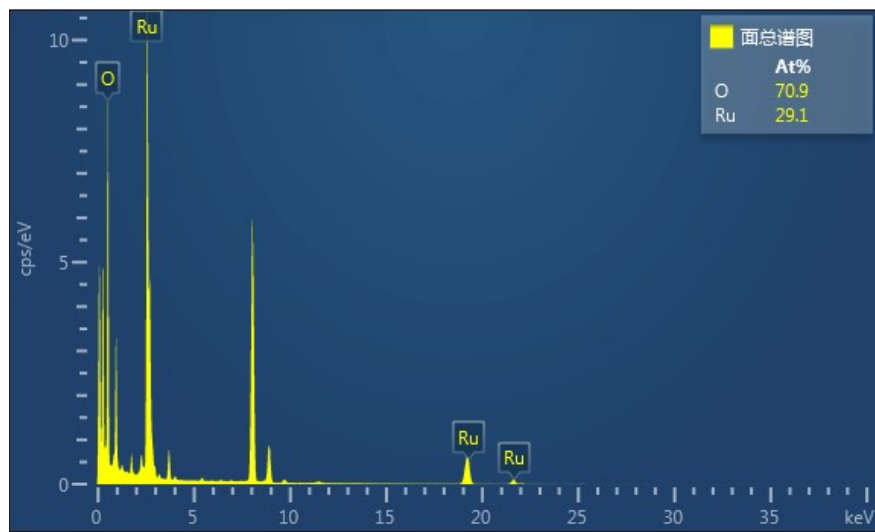


Fig. S2. The EDS pattern of the RuO_x.

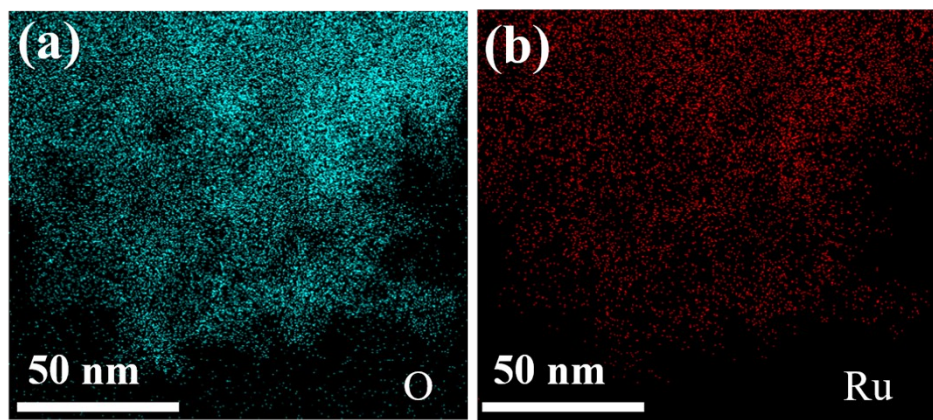


Fig. S3. EDS element mappings of O and Ru elements in the RuO_x.

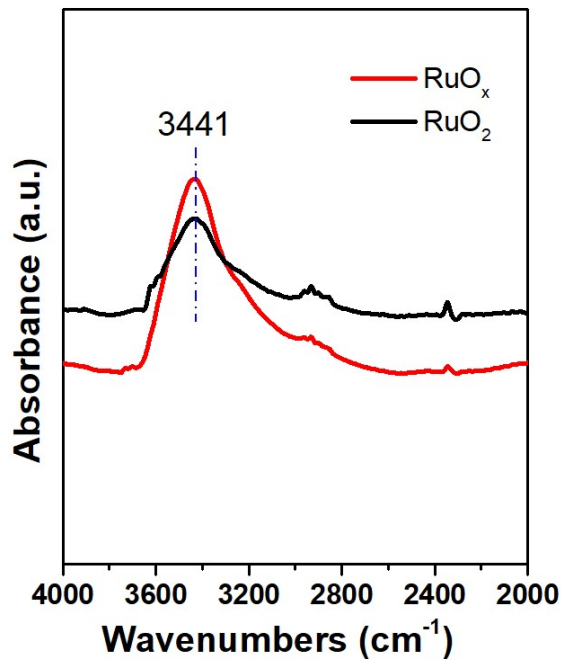


Fig. S4. FTIR images of the RuO₂ and RuO_x.

The FTIR spectra of the synthesized RuO₂ and RuO_x are presented in Fig. S4. A broad band between 3000 and 3700 cm⁻¹ is attributed to the stretching mode of hydrogen-bonded hydroxyl groups. Peak intensity of the FTIR adsorption ascribed to hydroxyl groups for the RuO_x is higher than that of the RuO₂, indicating that the RuO_x has the more surface hydroxyl groups than the RuO₂.

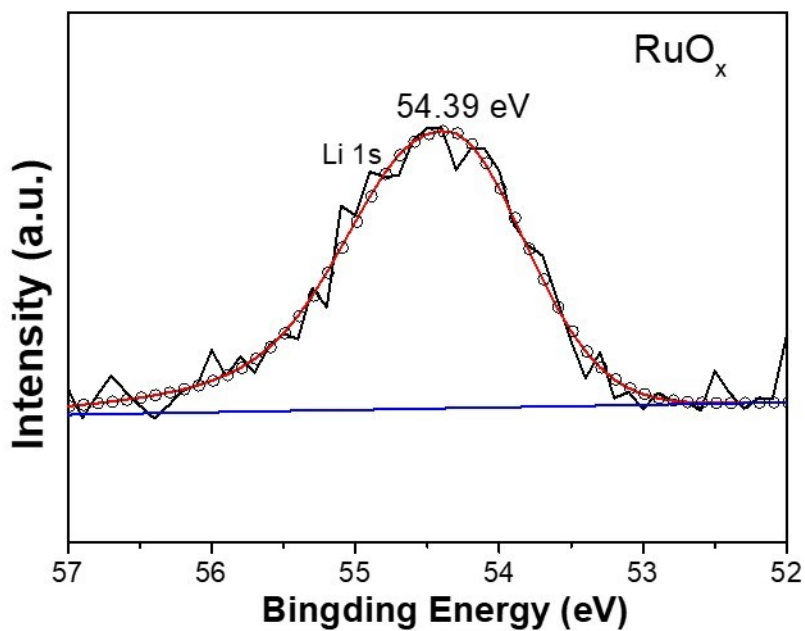


Fig. S5. High resolution XPS spectra for Li 1s of the RuO_x.

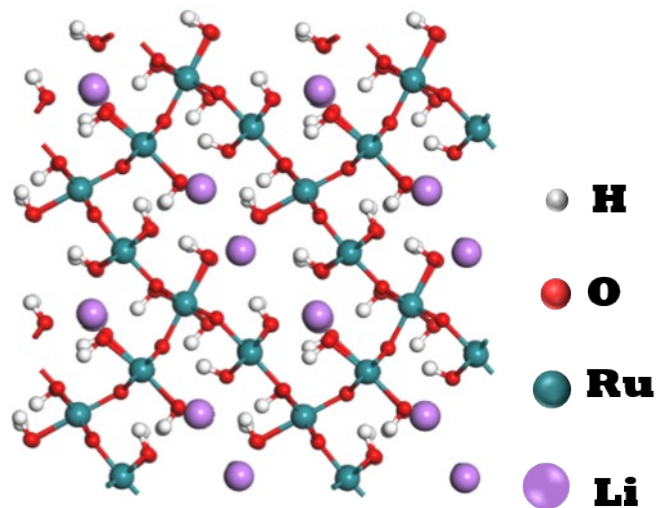


Fig. S6. The cell structure of the RuO_x.

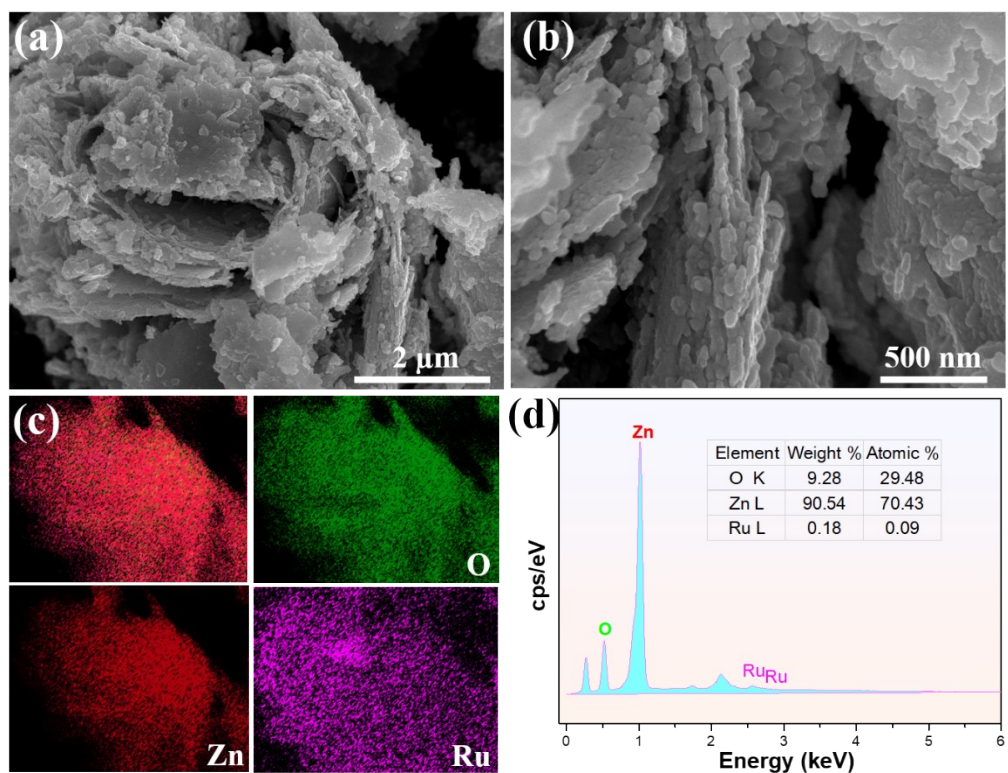


Fig. S7. (a,b) Typical FESEM images of ZnO/RuO_x with different magnification; (c) EDS element mappings of O, Zn and Ru; (d) the EDS patterns of ZnO/RuO_x.

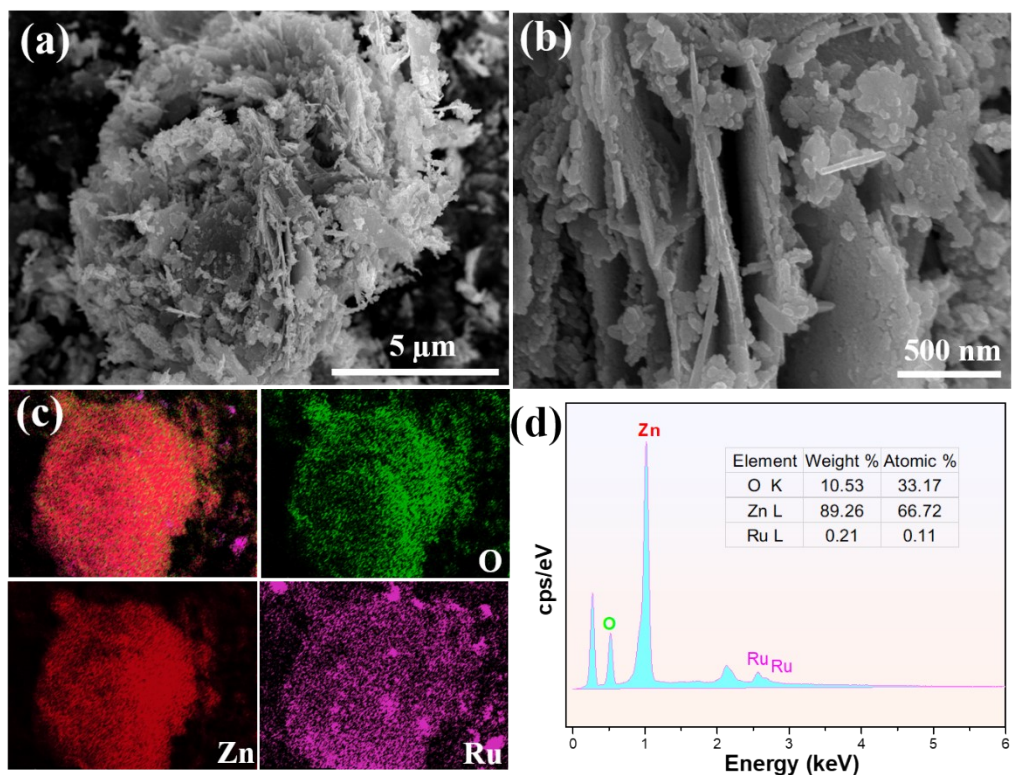


Fig. S8. (a,b) Typical FESEM images of ZnO/RuO₂ with different magnification; (c) EDS element mappings of O, Zn and Ru; (d) the EDS patterns of ZnO/RuO₂.

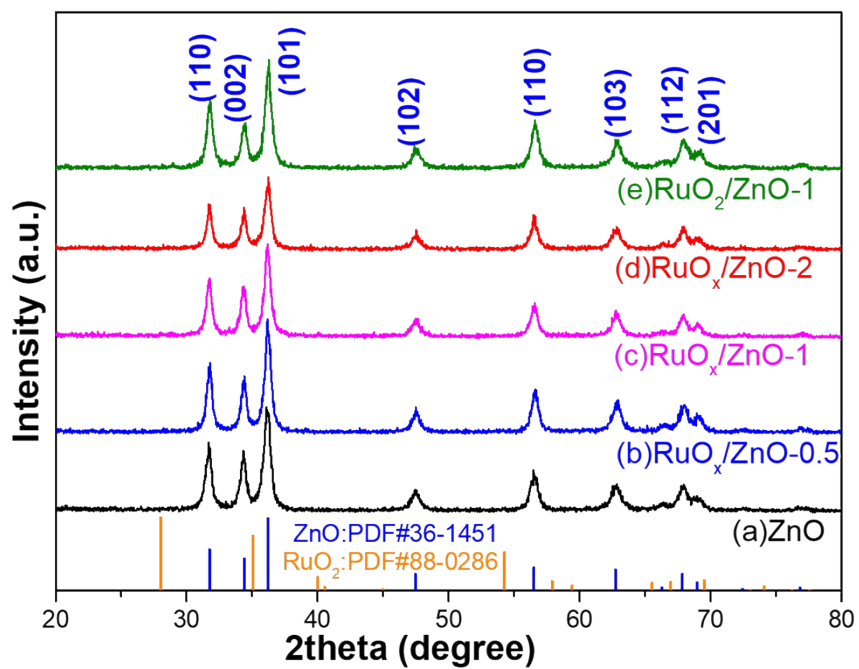


Fig. S9. XRD spectra for ZnO, RuO_x/ZnO-0.5, RuO_x/ZnO-1, RuO_x/ZnO-2 and RuO₂/ZnO-1.

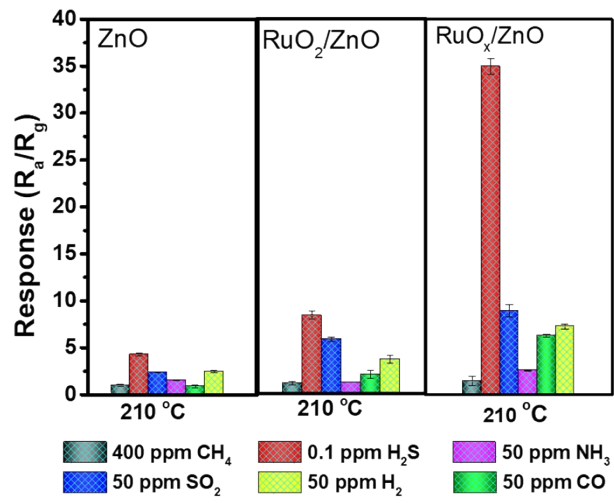


Fig. S10. The response of ZnO, RuO₂/ZnO and RuO_x/ZnO based sensors to various gas.

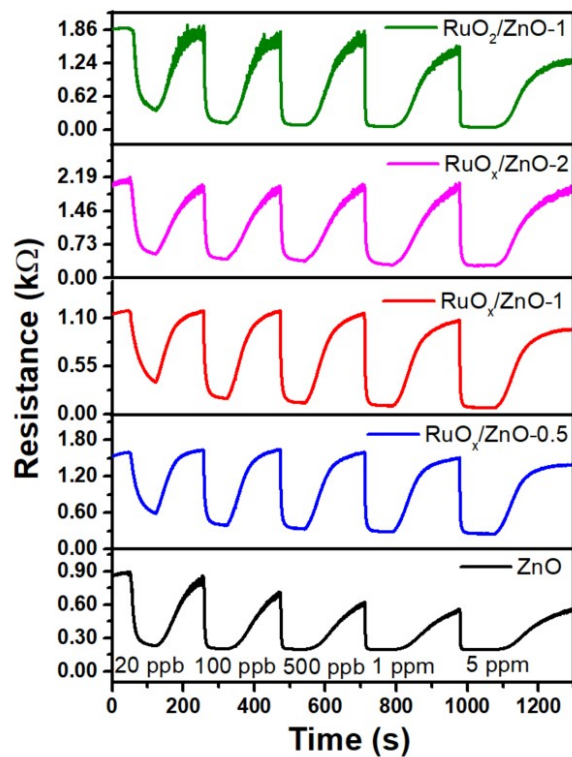


Fig. S11. Transient sensor resistance changes of the ZnO, RuO_x/ZnO-n ($n = 0.5, 1, 2$) and RuO₂/ZnO-1 sensors towards different concentrations (20 ppb-5 ppm) of H₂S at 210 °C.

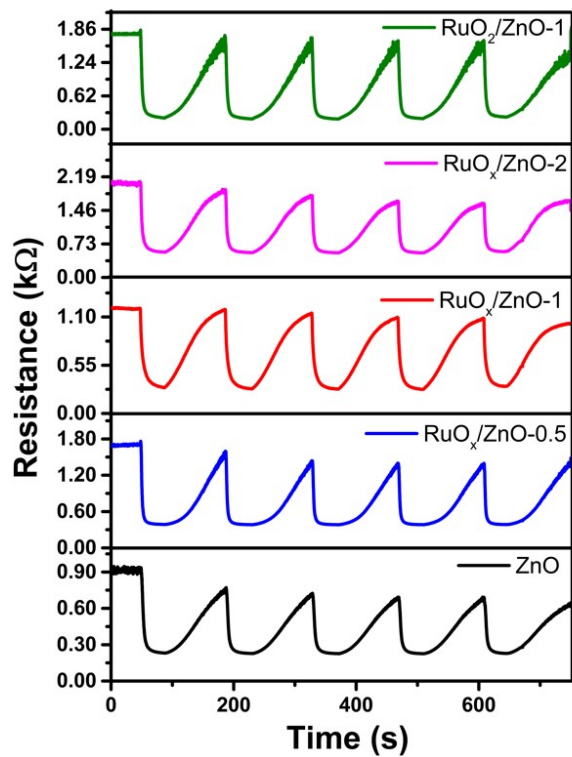


Fig. S12. Repeatability measurements of the ZnO, $\text{RuO}_x/\text{ZnO}-n$ ($n = 0.5, 1, 2$) and $\text{RuO}_2/\text{ZnO}-1$ sensors towards 100 ppb H_2S at 210 °C.

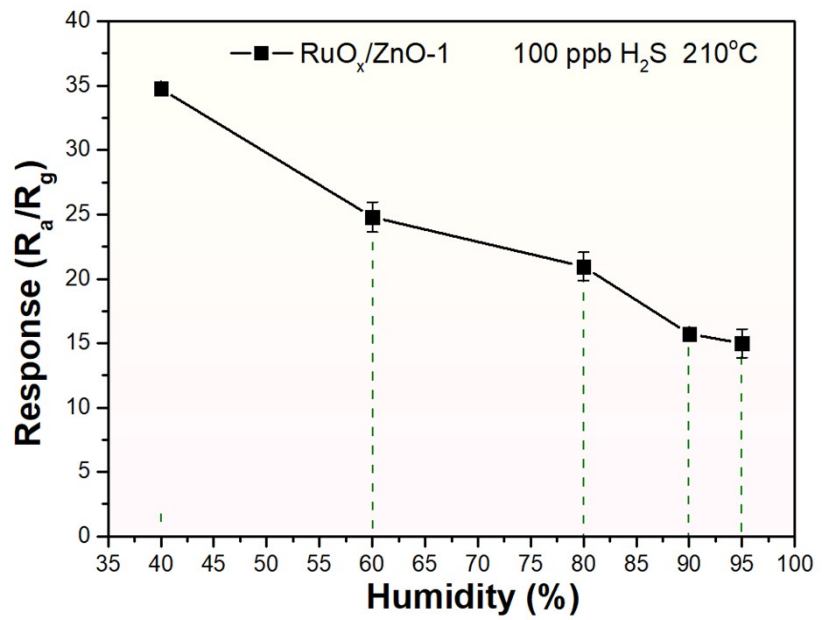


Fig. S13. The response of the $\text{RuO}_x/\text{ZnO}-1$ sensor under different humidity conditions.

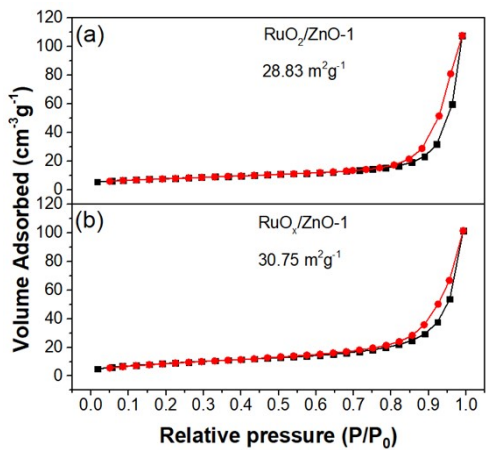


Fig. S14. N₂ adsorption-desorption isotherms of the RuO₂/ZnO-1 and RuO_x/ZnO-1.

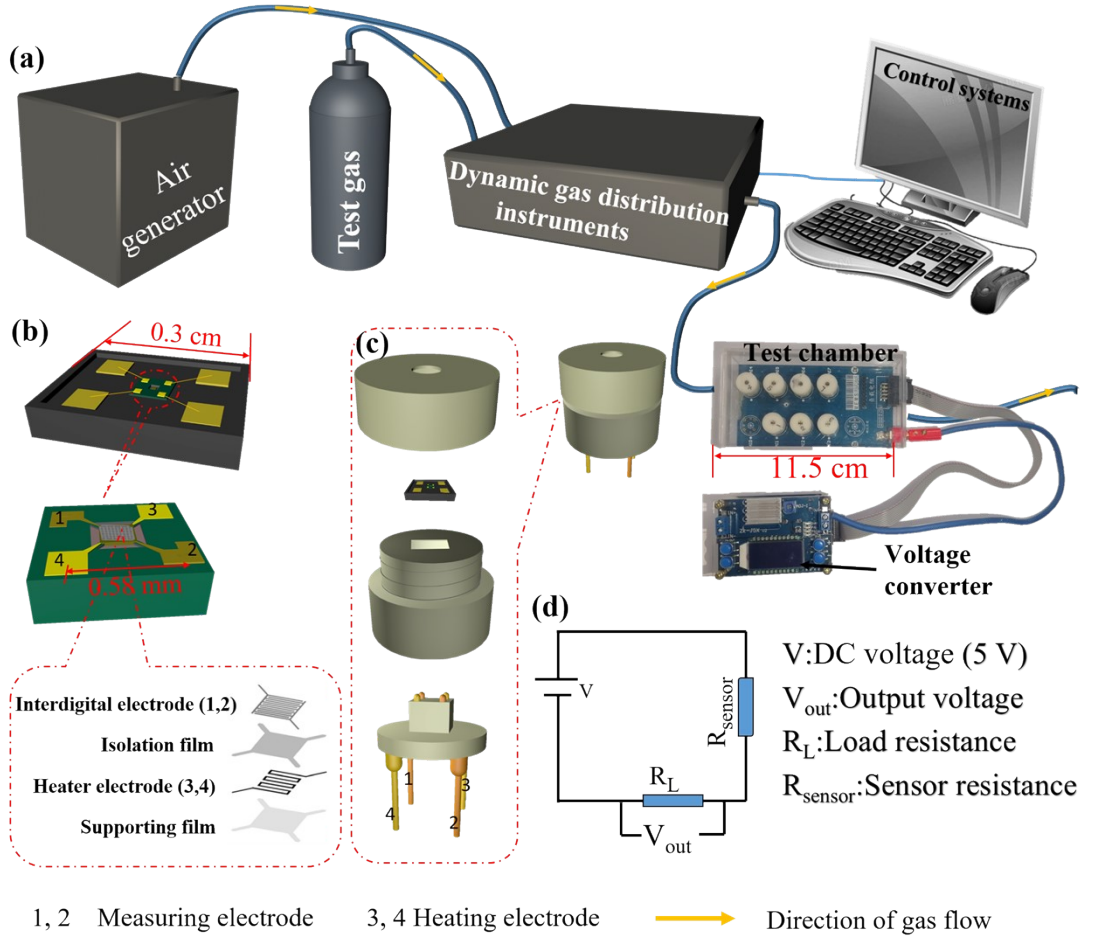


Fig. S15. (a) The test system of the MEMS gas sensor; (b) MEMS and exploded view of chip center area; (c) the exploded views of test base; (d) Measuring circuit of MEMS gas sensor.

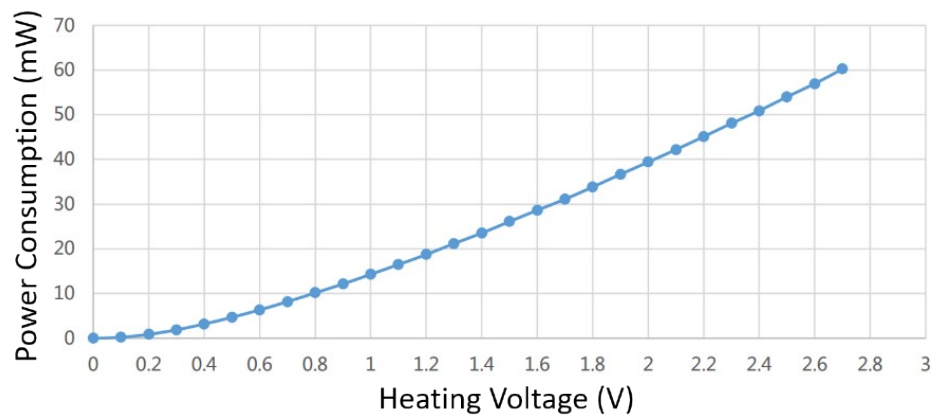


Fig. R16. The relations between the power consumption and heating voltage.

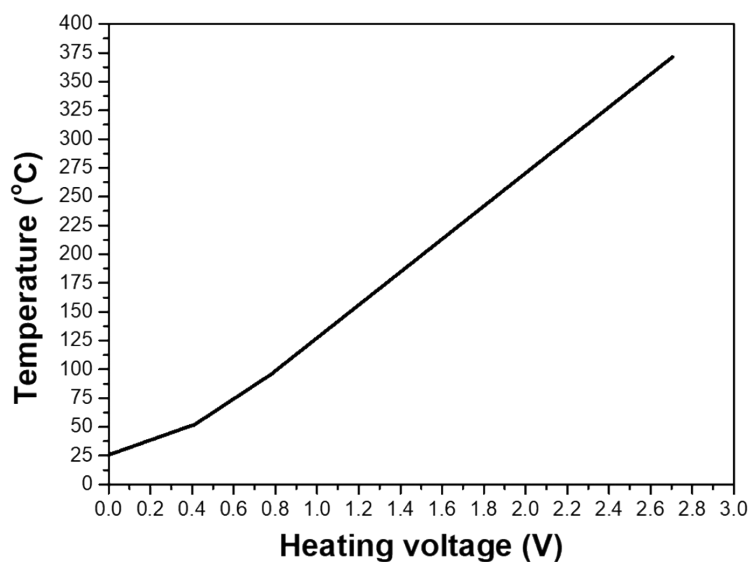


Fig. S17. The relationship between the heating voltage and the working temperature.

Table. S1 ICP-MS results of the RuO_x.

Sampling mass/g	Volume /ml	Dilution factor	Test element	Instrument reading	Unit	Conversion content	Unit	Mass fraction/%
0.0378	100	1	Li	2.614	mg/L	6915.34	mg/kg	0.691
0.0378	100	10	Ru	10.58	mg/L	279894.18	mg/kg	27.99

Table S2. Response (T_{res}) and recover (T_{rec}) time of the $\text{RuO}_x/\text{ZnO}-1$ sensor to different concentrations of H_2S at 210°C.

H_2S (ppm)	0.020	0.1	0.5	1	5
T_{res} (s)	11	8	8	7	6
T_{rec} (s)	42	40	40	38	37

Table S3. Comparison between the H₂S sensor in this work and reported work.

Materials	Concentration (ppm)	Response	Temperature (°C)	Response and recovery times		Limit of detection (ppb)	reference
				t _{Res} (s)	t _{Rec} (s)		
ZnO	0.1	4.27	210	12	50	20	This work
RuO ₂ /ZnO-1	0.1	13.42	210	10	45	20	
RuO ₂ /ZnO-1	0.1	35	210	8	40	20	
ZnO	100	15.92	150	65	2	1000	S1
Pd-loaded SnO ₂	20	~21	200	~30	~170	10	S2
ZnO-rGO	20	3.7	RT	404	275	8	S3
Net-like SnO ₂ /ZnO	5	112	100	-	513	10	S4
ZnO-CuO	10	72	115	~150	55	200	S5
Au/ZnO	3	475	25	11 min	20 min	0.5	S6
Mo-doped ZnO	5	14.11	300	~40	~50	250	S7
α-MoO ₃ /ZnO	0.5	4	270	13	29	500	S8
Pt /WO ₃	5	372	365	-	-	0.4	S9
Pt /SnO ₂	1	70	30	280	510	100	S10
Pt/SnO ₂	1	10.8	250	192.4	76.5	1000	S11
MoO ₃ /SnO ₂	10	43.5	115	22	10	100	S12
Au/ZnO/SnO ₂	1	73.3	350	36	786	100	S13

References:

- S1. S. Zhang, Z. Liu, L. Zhang, J. Chen, Q. Zhou, H. Zhang, L. Nie, Z. Dong, Z. Zhang, Z. Wang and G. Pan, *Chem. Phys. Lett.*, 2021, **763**, 138188.
- S2. Y. Su, P. Chen, P. Wang, J. Ge, S. Hu, Y. Zhao, G. Xie, W. Liang and P. Song, *RSC Adv.* 2019, **9**, 5987-5994.
- S3. A. D. Ugale, G. G. Umarji, S. H. Jung, N. G. Deshpande, W. Lee, H. K. Cho and J. B. Yoo, *Sens. Actuators B-Chem*, 2020, **308**, 127690.
- S4. D. Fu, C. Zhu, X. Zhang, C. Li and Y. Chen, *J. Mater. Chem. A*, 2016, **4**, 1390-1398.
- S5. Z. Cao, L. Gao, J. Mi, Y. Yuan, Q. Yang, Y. Luo, J. Shi and G. Duan, *ACS Appl. Nano Mater.* 2022, **5**, 2126-2136.
- S6. Z. S. Hosseini, A. Mortezaali, A. Iraji zad and S. Fardindoost, *J. Alloys Compd.* 2015, **628**, 222-229.
- S7. H.-S. Woo, C.-H. Kwak, I.-D. Kim and J.-H. Lee, *J. Mater. Chem. A*, 2014, **2**, 6412-6418.
- S8. H.-L. Yu, L. Li, X.-M. Gao, Y. Zhang, F. Meng, T.-S. Wang, G. Xiao, Y.-J. Chen and C.-L. Zhu, *Sens. Actuators B-Chem*, 2012, **171-172**, 679-685.
- S9. M.-H. Kim, J.-S. Jang, W.-T. Koo, S.-J. Choi, S.-J. Kim, D.-H. Kim and I.-D. Kim, *ACS Appl. Mater. Interfaces*, 2018, **10**, 20643-20651.
- S10. Y.-P. Sun, Y.-F. Zhao, H. Sun, F.-C. Jia, P. Kumar and B. Liu, *J. Alloys Compd.* 2020, **842**, 155813.
- S11. P. M. Bulemo, H. J. Cho, D. H. Kim and I. D. Kim, *ACS Appl. Mater. Interfaces*, 2018, **10**, 18183-18191.
- S12. X. Gao, Q. Ouyang, C. Zhu, X. Zhang and Y. Chen, *ACS Appl. Nano Mater.* 2019, **2**, 2418-2425.
- S13. C. M. Hung, H. V. Phuong, V. Van Thinh, L. T. Hong, N. T. Thang, N. H. Hanh, N. Q. Dich, N. Van Duy, N. Van Hieu and N. D. Hoa, *Sens. Actuators, A* 2021, **317**, 112454.